

# Rotation of actin monomers during isometric contraction of skeletal muscle

Julian Borejdo  
Priya Muthu  
John Talent  
Irina Akopova  
Thomas P. Burghardt

University of North Texas Health Science Center  
Department of Molecular Biology and Immunology  
Fort Worth, Texas 76107

and  
Mayo Clinic  
Department of Physiology and Biomedical  
Engineering  
Rochester, Minnesota 55905

**Abstract.** Cyclic interactions of myosin and actin are responsible for contraction of muscle. It is not self-evident, however, that the mechanical cycle occurs during steady-state isometric contraction where no work is produced. Studying cross-bridge dynamics during isometric steady-state contraction requires an equilibrium time-resolved method (not involving application of a transient). This work introduces such a method, which analyzes fluctuations of anisotropy of a few actin molecules in muscle. Fluorescence anisotropy, indicating orientation of an actin protomer, is collected from a volume of a few attoliters ( $10^{-18}$  L) by confocal total internal reflection (CTIR) microscopy. In this method, the detection volume is made shallow by TIR illumination, and narrow by confocal aperture inserted in the conjugate image plane. The signal is contributed by approximately 12 labeled actin molecules. Shortening of a myofibril during contraction is prevented by light cross-linking with 1-ethyl-3-[3-dimethylamino]propyl]-carbodiimide. The root mean-squared anisotropy fluctuations are greater in isometrically contracting than in rigor myofibrils. The results support the view that during isometric contraction, cross-bridges undergo a mechanical cycle. © 2007 Society of Photo-Optical Instrumentation Engineers. [DOI: 10.1117/1.2697286]

Keywords: isometric contraction; muscle; microscopy; total internal reflection; actin.

Paper 06103R received Apr. 18, 2006; revised manuscript received Aug. 7, 2006; accepted for publication Aug. 31, 2006; published online Mar. 2, 2007.

## 1 Introduction

Muscle contraction is caused by cyclic interaction of myosin heads with actin filaments driven by hydrolysis of ATP. The question arises whether, during steady-state isometric contraction (where no global work is produced), myosin heads perform a mechanical cycle at all. It is not at all obvious that they do. While the crystal structure of subfragment-1 (S1)<sup>1</sup> indicates a potential for large conformational change, and there is solid evidence that the C-terminal part of S1 rotates during translation of myosin along actin *in vitro*,<sup>2,3</sup> the situation may be quite different during steady-state isometric contraction of muscle. Under truly isometric steady-state conditions, the extent of the power stroke may be limited. In the extreme case, where there is no series elasticity, the rotation may be prevented altogether.<sup>4</sup> Moreover, muscle is a highly organized system characterized by a large concentration of contractile proteins.<sup>5</sup> The behavior of proteins *in vivo* may be different than *in vitro*, because in solution proteins are loosely packed, whereas *in vivo* they are crowded. Molecular crowding influences protein solubility and conformation in solution, which may impose constraints affecting both structure and function of enzymes.<sup>6,7</sup>

There are two ways of studying cross-bridge mechanics in muscle under isometric conditions. The first way is to use mechanical transient methods, during which a rapid step is applied to synchronize the cross-bridges, and to follow relaxation back to steady state.<sup>8–11</sup> The second way is to observe the dynamics of a few cross-bridges without disturbing the steady-state condition. In muscle the two ways are not equivalent. In transient methods, the rotation of cross-bridges is measured while they act against series elasticity, which is rapidly decreased following transient relaxation. In truly isometric contraction, however, series elasticity is constant and equal to active tension. This is a more accurate reflection of behavior of muscle proteins during isometric steady state.

It is thus preferable to study cross-bridge dynamics in isometric muscle by the passive time-resolved method. Conventional steady-state measurements are not time resolved.<sup>12–14</sup> This work introduces such a method. It is based on fluctuation analysis of rotational anisotropy. In fluctuation analysis, the signal-to-noise ratio (SNR) is proportional to  $N^{-1/2}$ , where  $N$  is the number of detected rotating molecules.<sup>15</sup> For this reason we seek to limit contributing molecules to just a few. The measurement from a few molecules in muscle is a complex task, because concentration of myosin or actin in muscle is large (e.g., a 1 cm long single muscle fiber contains  $\sim 10^{13}$  myosin molecules). To observe just a few molecules in muscle, it is necessary to decrease the number of active cross-

Address all correspondence to Julian Borejdo, Mol Biol, University of North Texas HSC, 3500 Camp Bowie Blvd, Fort Worth, TX 76107 United States of America; Tel: 817-735-2106; fax: 817-735-2118; E-mail: jborejdo@hsc.unt.edu

bridges, or to collect data from an extremely small volume. In earlier work, we adopted the first approach by poisoning or extracting myosin from fibers.<sup>16</sup> However, this led to complications due to modifications of enzymatic or structural properties of muscle. Here, we choose the second approach—to decrease the volume. The conventional wide-field microscope cannot be used for this purpose because its detection volume is much too large ( $\sim 10^{-9}$  L) containing  $\sim 10^{11}$  myosins. High aperture objectives forming diffraction-limited illuminated spots and confocal detection made it possible to limit the detection volume to  $\sim 0.5$  femtoliter ( $10^{-15}$  L) and eliminate much background,<sup>17</sup> but half of a femtoliter is still far too large to optically isolate just a few myosin molecules. The situation is not much improved by use of two-photon excitation.<sup>10</sup> It is necessary to reduce the volume at least 1000 times.

Attoliter detection volumes have recently been obtained utilizing evanescent field excitation. Zero-mode waveguides consisting of small apertures in a metal film deposited on a coverslip<sup>18</sup> limit the  $z$  dimension to the depth of an evanescent wave ( $\sim 100$  nm) and the  $x$  and  $y$  dimensions by the size of the aperture. However, the manufacture of film with small apertures is complex and expensive. Near-field scanning optical microscopy (NSOM) produces an evanescent field at the end of a tapered fiber optic tip that can be scanned over the sample surface. Excitation field dimensions are likewise on the order of 100 nm.<sup>19–21</sup> NSOM probes are expensive and must be near to (within 5 nm) a muscle fiber, or be inserted into it. This is difficult to accomplish without breaking a fragile NSOM fiber tip. Other techniques utilize the evanescent field produced at a glass/water interface by light undergoing total internal reflection (TIR). Light incident from the glass side of the interface at angles greater than the critical angle for TIR produce an evanescent field on the water side of the interface. In a microscope, the glass/water interface is formed by the coverslip/sample, and incident light may be introduced through the objective in a technique called prismless TIR.<sup>22</sup> Depth of focus is equal to the evanescent field depth ( $\sim 100$  nm). The  $x$  and  $y$  dimensions of the detection volume are limited by the confocal aperture inserted in the conjugated image plane. Several forms of confocal TIR (CTIR) have been described,<sup>23</sup> some having resolution on the order of a few attoliters.<sup>24,25</sup> An application utilizing CTIR and fluorescence correlation spectroscopy (FCS) has recently been described.<sup>26</sup> It is a modification of the CTIR method that we apply here to muscle. The method has never been applied before to the whole tissue.

In this work, we studied orientation changes of actin filaments labeled with fluorescent phalloidin. Phalloidin attaches to actin rigidly and rotates in synchrony with an interacting cross-bridge.<sup>27</sup> Studying actin rotation has four critical advantages.

1. Labeling of actin with phalloidin, in contrast to labeling myosin at Cys707, does not affect enzymatic properties of muscle.<sup>28,29</sup> Myofibrils are well preserved, because labeling does not require harsh conditions, such as raising the temperature to label myosin light chains.

2. Phalloidin labels the overlap zone.<sup>30</sup> Redistribution of phalloidin to the I-band takes several hours,<sup>31</sup> so only those

**Table 1** Composition of solutions. All solutions contained 10-mM Tris-HCl buffer pH 7.5. Contracting solution contained 20-mM phosphocreatine and 1-mg/ml creatine kinase.<sup>54</sup> The glycerinating solution contained 80-mM K-acetate, substituted for KCl, and 0.2-mg/ml PMSF, 2-mM mercaptoethanol, and 50% glycerol. All solutions contained a deoxygenating system of 4.5-mg/ml mg glucose, 216- $\mu$ g/ml glucose oxidase, and 36- $\mu$ g/ml catalyze.<sup>46</sup> Concentrations in mM.

Solution	MgCl <sub>2</sub>	CaCl <sub>2</sub>	EGTA	EDTA	ATP	KCl	DTT
EGTA-rigor	4		2			50	1
EDTA-rigor				2		50	1
Ca <sup>2+</sup> -rigor	4	0.1				50	1
Contracting	4	0.1			5	50	1
Glycerinating	2		5		5	See above	2

actin protomers that are located in the region where interactions with myosin occur are studied.

3. By saturating all actins with a mixture of labeled and unlabeled phalloidins, the final concentration of label is easily controlled. For example, in the present experiments we used 0.01- $\mu$ M fluorescent phalloidin and 9.99- $\mu$ M unlabeled phalloidin, i.e., we could be sure that on average only 1 in 1000 actin monomers in a thin filament carried a fluorescent probe.

4. Fluorescence of phalloidin increases on binding to actin.<sup>29</sup> This increases SNR.

To avoid shortening during contraction, myofibrils were lightly cross-linked with 1-ethyl-3-[3-dimethylamino]propyl]-carbodiimide (EDC). The results support the view that during isometric contraction, cross-bridges undergo mechanical cycles.

## 2 Materials and Methods

### 2.1 Preparation

#### *Chemicals and solutions.*

5'-iodoacetamido-tetramethyl-rhodamine (5'-IATR or Rh) was from Molecular Probes (Eugene, Oregon). 1-ethyl-3-[3-dimethylamino]propyl]carbodiimide (EDC), phosphocreatine, creatine kinase, glucose oxidase, and catalyze were from Sigma (Saint Louis, Missouri). Composition of various solutions is shown in Table 1.

*Preparation of myofibrils.* Muscle was washed with cold EDTA-rigor solution for 1/2 hr followed by Ca-rigor solution. Myofibrils were made from muscle in Ca-rigor as described before.<sup>13</sup>

*Cross-linking of myofibrils.* To prevent shortening during contraction, myofibrils were lightly cross-linked with water-soluble cross-linker EDC.<sup>32</sup> 1-mg/ml myofibrils were incubated with 2-mM EDC for 10 min at room temperature. The reaction was stopped by 20-mM DDT. The lack of shortening was checked in a phase microscope.

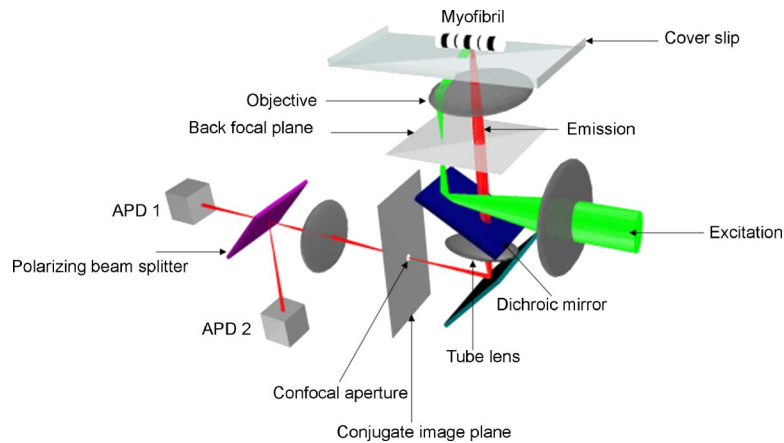


**Fig. 1** Prismless confocal total internal reflection (CTIR) microscope. 532-nm light is totally internally reflected at the surface of the coverslip. Fluorescent light emitted by muscle is collected by the objective onto a tube lens, which focuses it on a conjugate image plane. A confocal aperture is inserted at this plane. The polarized fluorescence intensities are detected by Avalanche Photodiodes (APD).

*Preparing the sample.* Number 1 cover slips (20×60 mm) (Corning, New York) were cleaned with 90% ethanol. A narrow channel was created by applying a thin layer of Vaseline along the edges of the cover slip. 25  $\mu\text{L}$  of sample was applied to the cover slip by streaking the pipette along the long axis (to align, as much as possible, the myofibrils with the long axis of the cover slip) and left for 3' to allow myofibrils to adhere to the glass. The long cover slip was covered with a small (20×20 mm) cover slip and washed with Ca-rigor solution by applying the solution to one end of the channel and sucking with number 1 filter paper at the other.

*Measuring ATPase activity.* Myofibrillar ATPase activity was measured using an Inorganic Phosphorus Reagent Kit (Pointe Scientific, Canton, Ohio); reaction was initialized by adding 5-mM ATP to 50  $\mu\text{L}$  of 3-mg/ml myofibrils in Ca-rigor solution. Myofibrils were intensively shaken during 1-min incubation at room temperature. Reaction was stopped with 0.95 ml of Pi-reagent, filtered through a 1-ml pipette tip closed with a cotton ball and dissolved in 2-mM SDS. Concentration of [Pi] in  $\mu\text{M}$  was calculated as  $A_{\text{sample}} \cdot 10/A_{\text{standard}}$ , where  $A_{\text{standard}}=0.34$  is the absorption of a standard sample of 10- $\mu\text{M}$  Pi.

## 2.2 Instrument

The principle of the CTIR method is illustrated in Fig. 1. Excitation light from an expanded DPSS laser beam (Compass 215M, Coherent, Santa Clara, California) enters the epillumination port of the inverted microscope (Olympus IX51). The expanded laser beam, focused at the back focal plane of the objective, is directed by the movable optical fiber adapter to the periphery of the objective (Olympus PlanApo 60×, 1.45 NA), where it refracts and propagates toward the glass/buffer interface at incidence angles greater than the critical angle  $\theta_c$ . Excitation light totally internally reflects at the interface and produces an evanescent wave on the aqueous side of the interface.<sup>33</sup> Exciting light was s-polarized (perpendicular to the incidence plane) giving an evanescent field similarly linearly polarized.<sup>34</sup> Fluorescence was always excited with linearly polarized light parallel to the myofibrillar axis. The evanescent field decays exponentially in the  $z$  dimension with

a penetration depth  $d=\lambda_0/[4\pi(n_g^2\sin^2\theta-n_w^2)^{1/2}]$ , where  $\lambda_0$  is the wavelength of the incident light,  $n_g$  ( $=1.5$ ) is glass refractive index, and  $n_w$  ( $=1.33$ ) is the refractive index of water. Despite the higher refractive index of the fiber ( $\sim 1.37$ ), TIR occurs where the glass substrate meets the fiber, because the incident angles utilized are  $>70$  deg (objective numerical aperture=1.45). The sample rests on a movable stage (model 426A, Newport, Irvine, California) actuated by a servo motor (model LTA-HL, Newport) driven by a motion controller (model ESP300, Newport). This provides 40-nm incremental motions, small enough to place a myofibrillar A-band in a position conjugate to the aperture. The fluorescent light is collected through the same objective and projected onto a tube lens, which focuses it at the conjugate image plane (10.2 cm away from the side surface of the microscope). A confocal aperture or an optical fiber (whose core acts as a confocal aperture) is inserted at this plane. The exact  $z$  position of the aperture does not much matter for high power objectives (because back focal length is large), and is adjusted by a zoom housing (Thor Laboratories, Newton, New Jersey, SM1ZM). The  $xy$  position of aperture is adjusted by the  $xy$  translator (Thor Laboratories, ST1XY). The fluorescent light emerging from the aperture is projected to a polarizing beam-splitter located at the center of custom-made fluorescence cell (Quantum Northwest, Spokane, Washington). Light is collected by a pair of Avalanche Photodiodes (APD, Perkin-Elmer, Norwalk, Connecticut, SPCM-AQR-15-FC).

The well-defined polarization of exciting light is crucially important in the proposed experiments. For this reason, the coupling must be done through a polarization preserving single-mode optical fiber. Those fibers have small diameters ( $\sim 3$   $\mu\text{m}$ ) and are difficult to couple efficiently with the laser beam. We used a commercial fiber (kineFlex, PointSource, England) mounted into a kinematic adapter (model KC1, Thor, Newton, New Jersey) to assure reasonably high coupling efficiency ( $\sim 50\%$ ), i.e., we can launch  $\sim 25$  mW of 532-nm light into a TIRF module.

## 2.3 Photon Counting

Each polarized component is detected by a separate avalanche photodiode. The APD quantum efficiency is  $\sim 65\%$  at

500 nm, the dark count is  $\sim 10$  cps, and it can count up to  $10^7$  counts/sec. The APD's TTL pulses are counted by counter/timers on an interface card (model 6601, National Instruments, Austin TX) controlled by a custom LabView program. Photon counting eliminates the need for a frame grabber and allows direct 16-bit counting by a PC. The board counts intensities as follows: four counter/timers on the NI 6601 card are utilized, two as event counters to detect TTL pulses from the APDs, another as a clock, and a fourth as a pulse generator. The event counters operate in buffered mode to ensure continuous data acquisition. In this mode, counters are read "on the fly" with sampling rates approaching 1 MHz. The two counters, the clock, and the pulse generator are gated active simultaneously by a shutter pulse to begin data acquisition. Counters are read simultaneously at the rising edge of the clock.

#### 2.4 Choice of Sampling Time

Bin width is defined as the time interval by which the data collection time is subdivided. The necessary data collection time is determined by the characteristic time for hydrolysis, i.e.,  $\sim 0.5$  sec.<sup>35</sup> During this time, we wish to measure at least five data points, i.e.,  $\delta\tau \sim 100$  msec.

### 3 Results

#### 3.1 Size of the Observed Volume

Fluorescent intensity at the microscope image plane is the convolution of the excitation and emission intensity profiles.<sup>36</sup> The light intensity profiles are derived from geometrical optics and given by the Fraunhofer diffraction patterns from a circular aperture.<sup>37</sup> Detected fluorescence is the intensity at the image plane integrated over the confocal pinhole. Thus the size and shape of the detection volume depends on the excitation beam profile, diffraction of emitted light through the microscope optics, and the size and shape of the confocal pinhole.

In CTIR, the spatial distribution of the excitation field intensity decays exponentially in the dimension normal to the glass/water interface ( $z$  dimension) and is uniform in the lateral ( $xy$ ) dimensions. The point spread function integrated over the pinhole aperture in image space (integrated PSF or IPSF) as a function of point source position sets boundaries for the detection volume appropriate for a point-like diffusing fluorescent sphere. Figure 2(a) shows the IPSF for a NA-1.45,  $60\times$  objective and a  $3.5\text{-}\mu\text{m}$  confocal pinhole as a function of point source position in the object plane ( $xy$  plane on the water side of the interface). Figure 2(b) shows the IPSF for the same objective and pinhole, but for the point source position in an axial plane ( $yz$  plane on the water side of the interface). The  $z$  dimension dependence is exponential with a depth of field of  $\sim 100$  nm.

We calculate the effective detection volume by deploying a rectangular solid lattice of identical chromophores in the object space. The lattice fills the volume occupied by water and sample in a real experiment. A single chromophore, the principal chromophore, occupies the point of maximum intensity of the IPSF in Fig. 2. Fluorescence detected from each chromophore is summed and normalizes fluorescence collected from the principal chromophore as a function of the unit cell

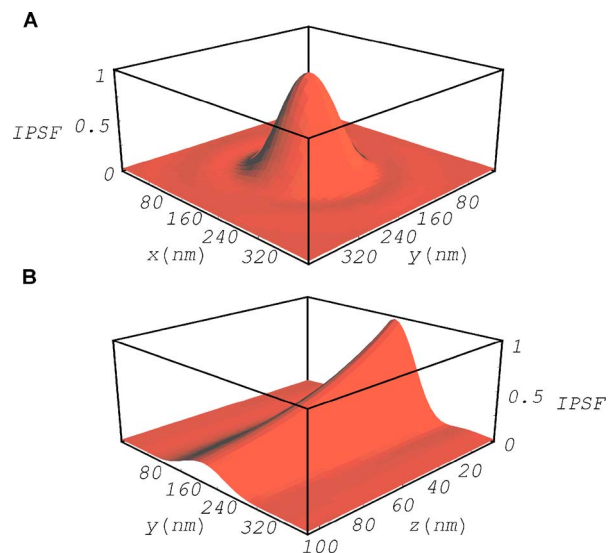


**Fig. 2** The calculated relative detected intensity from a point-like fluorescent sphere (FS) near the focus of a NA-1.45,  $60\times$  objective as a function of FS position in lateral ( $x, y$ ) and axial coordinates ( $z$ ). Calculation utilizes the point spread function integrated over the  $3.5\text{-}\mu\text{m}$  confocal pinhole aperture to give the integrated point spread function or IPSF. (a) is the IPSF for lateral FS position. (b) is the exponentially decaying IPSF for the axial FS position. The IPSF defines the effective detection volume using arguments outlined in the text. For this IPSF, the effective detection volume is  $\sim 7$  attol.

lattice dimensions. We elect to define the minimum unit cell volume as those dimensions, where the principal chromophore fluorescence accounts for more than half of the total fluorescence collected. The IPSF shown in Fig. 2 has a minimum unit cell with  $xyz$  dimensions of  $186 \times 186 \times 86$  nm. Four unit cells surround the principal chromophore defining the void to be filled by the effective detection volume. IPSF symmetry suggests that the void be filled with the largest possible ellipsoid forming the effective detection volume of  $\sim 7$  attol. This estimate was experimentally tested in work described elsewhere.<sup>38</sup>

#### 3.2 Determining the Position of the Conjugate Area

In experiments on muscle, it is important to place the A-band of myofibrils exactly at the sample plane position that is conjugate to the detector. To determine the exact position of conjugate area, a sharp edge was translated through a projection of  $3.5\text{-}\mu\text{m}$  aperture onto the sample plane. A razor edge was mounted on the moveable stage driven by a servo motor. To determine the  $y$  coordinate, the edge was translated in the  $x$  direction in  $0.1\text{-}\mu\text{m}$  steps. Light was detected only when the edge was near the line defined by the  $y$  coordinate. To determine the  $x$  coordinate, the edge was translated in the  $y$  direction along the line defined previously by the  $y$  coordinate. Figure 3 shows a contour map of the normalized intensity profile when the edge was translated in  $x$  and  $y$  directions. Red and violet colors correspond to the maximal and minimal intensity of transmitted light, respectively. The intersection of the profile lines defines a position of conjugate area with respect to the center of the eyepiece reticle. The coordinates of this area were  $x=1\text{ }\mu\text{m}$ ,  $y=1\text{ }\mu\text{m}$ . The A-band was placed within this area.

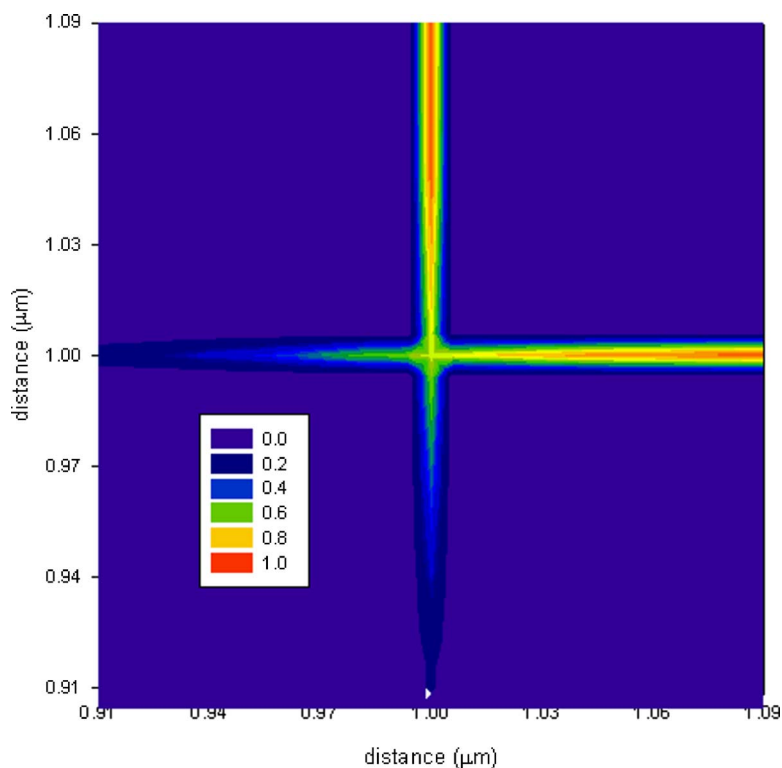


**Fig. 3** Defining area on the sample plane conjugate to the image plane. Contour map of the normalized intensity profile of the sharp edge translated in  $x$  and  $y$  directions in  $0.1\text{-}\mu\text{m}$  steps. Red and blue colors correspond to the maximal and minimal intensity of transmitted light, respectively. The intersection of the profile lines defines the position of the conjugated area relative to the center of the eyepiece reticle. (Color online only.)

### 3.3 Measuring Total Internal Reflection Fluorescence Polarizations

We measured the polarized fluorescence of standard samples with known polarizations and compared it with polarization obtained with TIRF illumination. The sample was poly(vinyl alcohol) (PVA) film doped with *N*-methyl-4-(pyrrolidinyl)-styrylpyridinium iodide (MPSPI) dye, in which transition dipoles are aligned in one direction by stretching the PVA film during polymerization (sample was provided by Dr. I. Gryczynski). MSPSI has a large Stokes shift and high polarization across absorption and emission spectra. The elongated shape of MSPSI allows for good orientation in stretched samples. Figure 4 shows the signal from a typical film. Polarization values are listed in Table 2. Horizontal and vertical (EPI) polarizations were comparable to the values obtained by a dedicated apparatus using a low numerical aperture (0.15) objective<sup>39</sup> ( $P_{\parallel}=0.903\pm 0.003$  and  $P_{\perp}=-0.630\pm 0.005$ , respectively), consistent with the value reported earlier.<sup>40</sup>

The other samples with known polarizations were rhodamine B in 100% glycerol (theoretical  $P=0.5$ , observed  $P=0.501$ ), unstretched (immobile) PVA doped with rhodamine B (theoretical  $P=0.5$ , observed  $P=0.333$ ), and rhodamine B in water (theoretical  $P=0.056$ , observed  $P=0.111$ ). The deviation from the ideal value is caused by unequal sensitivity of APDs and by the microscope optics. The fact that conventional and TIRF polarizations are similar is consistent with earlier work.<sup>41</sup>

### 3.4 Number of Observed Actin Monomers

We used  $0.01\text{-}\mu\text{M}$  fluorescent phalloidin+ $9.99\text{-}\mu\text{M}$  unlabeled phalloidin. Since there are  $\sim 400$  actin protomers in a filament, there is on average  $\sim \frac{1}{2}$  phalloidin molecule per actin filament. If the phalloidin was uniformly distributed,  $0.3\text{-}\mu\text{m}$ -wide detection volume would have contained  $\sim 0.2$  phalloidins/filament. However, because of nonhomogeneous distribution of phalloidin, most of the fluorophores are located in distal  $\sim 1/3$  of a filament. We therefore detect a signal from  $\sim 1$  phalloidin/filament. Spacing between actin filaments is  $\sim 30\text{ nm}$ .<sup>5</sup> Since the thickness of the detection volume is  $\sim 100\text{ nm}$ , we observe approximately three layers of thin filaments. There are approximately four filaments in each layer. We conclude that we observe  $\sim 12$  actin monomers labeled with phalloidin.

To verify this number experimentally, we constructed a calibration curve relating the intensity of fluorescence to the number of molecules contributing to a signal.  $1\text{-mg/mL}$  myofibrils were labeled for 5 min at room temperature with a mixture containing  $0.01\text{-}$ ,  $0.05\text{-}$ ,  $0.1\text{-}$ , or  $0.5\text{-}\mu\text{M}$  rhodamine-phalloidin complemented with  $9.99\text{-}$ ,  $9.95\text{-}$ ,  $9.90\text{-}$ , and  $9.5\text{-}\mu\text{M}$  unlabeled phalloidin, respectively. Assuming that actin is distributed continuously throughout the experimental volume, the number of rhodamine-phalloidin molecules in  $7\text{-attoL}$  volume is 4, 20, 40, and 200 for myofibrils labeled with  $0.01\text{-}$ ,  $0.05\text{-}$ ,  $0.1\text{-}$ , and  $0.5\text{-}\mu\text{M}$  rhodamine phalloidin,

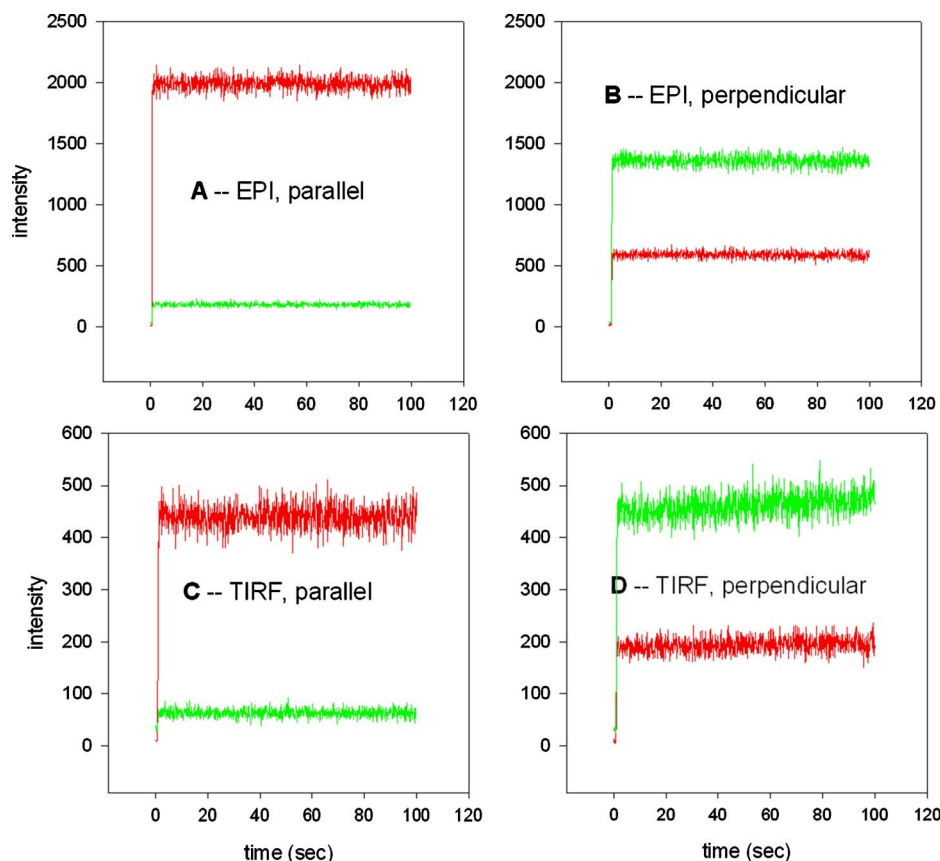


**Fig. 4** Polarization signal obtained from oriented PVA film. (a) Polarization of the excitation laser beam parallel to the axis of the film, emission parallel (dark gray) and perpendicular to the axis of the film (light gray); (b) Polarization of the excitation laser beam perpendicular to the axis of the film, with the same emission colors as before. (c) and (d) are the same as in (a) and (b) with TIRF excitation, laser beam at  $\sim 69$  deg to the plane of the film. The excitation intensity was attenuated 1000 times (to  $25 \mu\text{W}$ ).

respectively. The average number of photon counts of parallel polarized intensity was measured for each concentration of the dye. The result is shown in Fig. 5. The number of observed molecules was estimated from this calibration curve by measuring the average fluorescence emanating from the labeled sample. In general, the number varied between 4 to 20 fluorescent actin monomers.

The data of Fig. 5 allow us to estimate signal-to-noise ratio (SNR) in our experiment. The SNR is determined by the rate of detection of fluorescent photons per molecule of the dye during one bin width  $\delta\tau$ .<sup>42</sup> We detected on average  $\sim 2.5$  counts/bin/molecule for a parallel component of polarization signal. The perpendicular component is  $\sim 0.8\times$  parallel com-

ponent, giving a total of  $\sim 4$  photons/molecule/bin. Assuming Poisson distributed shot noise as the sole noise source, the SNR is  $\sim 2$ .

### 3.5 Fluctuations of Contracting Myofibrils

Myofibrils were placed on a cover slip and thoroughly washed with Ca-rigor. The flow removes free-floating myofibrils and those that are weakly attached to the glass, leaving only those that are strongly adhering to the top or bottom surfaces. A myofibril attached to the bottom surface is shown in Fig. 6(a). To visualize the size of the confocal aperture, the fifth sarcomere from the bottom was magnified  $10\times$  and is shown in Fig. 6(b). The projection of  $4\text{-}\mu\text{m}$  aperture onto the sample plane is shown as a black dot. The schematic diagram of detection volume is shown in Fig. 6(c).

Typical signals obtained from the detection volume placed in the overlap zone of rigor and contracting myofibril are shown in Figs. 7(a) and 7(b), respectively. Orthogonal fluorescence intensities decrement in time due to rhodamine photobleaching. The bleaching resulted in loss of all signal within  $\sim 50$  to  $60$  sec. The background was  $\sim 50$  cpb. It is due to the autofluorescence from glass, and could be decreased  $\sim 2$ -fold by using quartz coverslips; however, we found this approach impractical and used glass coverslips throughout. The time course of polarization ratio for rigor and active myofibrils was

**Table 2** Polarizations of samples. Polarization of solid PVA film doped with MPSPI dye, in which transition dipoles are aligned in one direction by stretching the PVA film during polymerization. The average horizontal and vertical polarizations are defined as  $P_{\parallel} = (F_{\parallel} - F_{\perp}) / (F_{\parallel} + F_{\perp})$  and  $P_{\perp} = (F_{\perp} - F_{\parallel}) / (F_{\perp} + F_{\parallel})$ , where  $F_{\parallel}$  and  $F_{\perp}$  are fluorescence intensities obtained with light polarized parallel and perpendicular to the muscle axis.

Sample	$P_{\parallel}(\text{EPI})$	$P_{\perp}(\text{EPI})$	$P_{\parallel}(\text{TIRF})$	$P_{\perp}(\text{TIRF})$
Oriented film	0.834	-0.396	0.749	-0.409

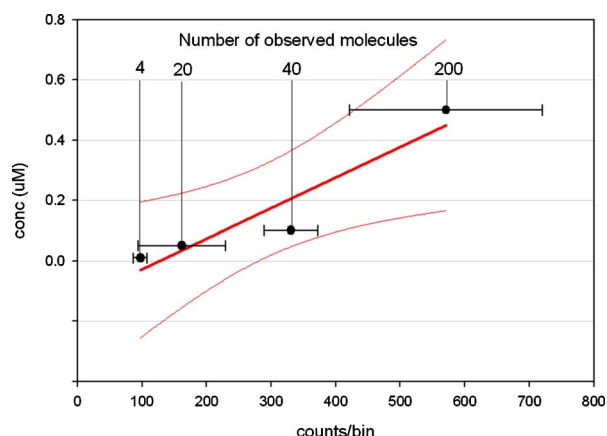


**Fig. 5** The calibration curve (thick line) used to estimate the number of fluorescent cross-bridges in the detection volume. The horizontal axis is the average  $\pm$  SEM intensity of the parallel intensity component of a fluorescence signal. The vertical axis is the corresponding concentration of fluorophores. The numbers point to the calculated number of fluorescent molecules in the detection volume. The thin lines denote 95% confidence limits.

formed using the formula  $P_{\parallel} = (F_{\parallel} - F_{\perp}) / (F_{\parallel} + F_{\perp})$ . A best fitting line is subtracted from each time course to remove the zero frequency (dc) component of its power spectrum, leaving time courses that have zero mean polarization ratio (the ac component or  $P_{ac}$ ) and fluctuations characterized by the root mean squared (rms) deviation  $(\langle \Delta P^2 \rangle)^{1/2}$ .

We investigated frequency dependence in the polarization fluctuations with the power spectrum (PS) computed from  $P_{ac}$  using fast Fourier transform (FFT) with a Bartlett window (Mathematica, Wolfram Research, Champaign, Illinois).

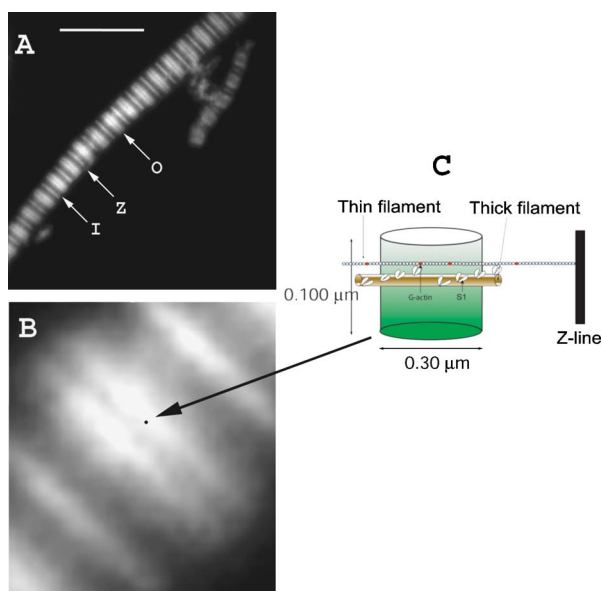


**Fig. 6** TIRF image of myofibril in rigor. (a) Myofibril labeled with 0.1- $\mu$ M fluorescein phalloidin on actin filaments. Z is the Z line, O is the overlap zone, and I is the I-band. The bar is 10  $\mu$ m. (b) Fluorescent image magnified 10 $\times$ . The black dot is a projection of the confocal pinhole on the image plane. (c) Schematic diagram of the voxel. The fluorescently labeled actin monomers are gray.

Spectral intensities were binned in 0.5-Hz intervals. The difference PS, constructed by subtracting rigor PS from active PS, defines excess PS from active myofibrils. Excess PS characterizes the rate of orientation change of the phalloidin transition dipole. Average excess PS computed from 23 myofibrils along with error bars indicating standard error of the mean ( $n=23$ ) is shown in Fig. 8 (top). The average excess PS was  $>0$  at every frequency detected and relatively flat. A paired two-sided t-test shows that excess PS differs significantly from zero (i.e.,  $P \leq 0.05$ ) at every frequency (Fig. 8, bottom).

The ATPase of uncrosslinked myofibrils was  $f_{ATP} = 131 \pm 2 \mu\text{mole Pi} / \mu\text{mole myosin/min} = 2.2 \text{ Hz}$ . Cross-linking increased ATPase of uncross-linked myofibrils  $1.2 \pm 0.07$  fold.

### 3.6 Controls

#### 3.6.1 Movement artifact

We have considered the possibility that the difference between contracting and rigor muscle is due to the movement artifact, i.e., that the cross-linking was not sufficient to inhibit shortening. To make sure that this was not the case, myofibrils were always tested for shortening after cross-linking. Figure 9 shows a typical example of two fluorescent images of the same myofibril in rigor [Fig. 9(a)], and a few minutes after adding contracting solution [Fig. 9(b)]. The mean  $\pm$  SD sarcomere length of rigor and contracting myofibrils was  $2.77 \mu\text{m} \pm 0.14 \mu\text{m}$  and  $2.78 \mu\text{m} \pm 0.12 \mu\text{m}$ , respectively. The paired t-test showed that the difference was not statistically significant ( $t=0.42$ ,  $P=0.68$ , 8 deg of freedom).

#### 3.6.2 Degree of cross-linking

To rule out the possibility that cross-linking affects polarized fluorescence, we measured the degree of cross-linking. Cross-linking increased ATPase of myofibrils  $1.2 \pm 0.07$  fold. In solution, cross-linking of skeletal rabbit S1 to F-actin accelerates ATPase 200 to 300 fold,<sup>43</sup> suggesting unlabeled cross-linked myofibril preparation contains 1 to 2% cross-linked cross-bridges.

## 4 Discussion

The main finding of this work is that actin monomers rotate during isometric contraction of myofibrils. Since rotation of actin is a result of interaction with myosin heads,<sup>27</sup> the present results suggest that cross-bridges rotate during isometric contraction, just like *in vitro*<sup>44</sup> or during translation along actin filaments.<sup>2</sup> We recognize that rotation of the head does not necessarily mean that the C-terminal part of myosin undergoes power stroke, because the C-terminal part is separated from the head by a flexible link.<sup>45</sup> Resolution of the question of rotation of the C-terminal part must wait until the CFTIR method is applied to myosin labeled at the tail.

We excluded four possible reasons why observed fluctuations could be artifactual.

1. *The spectra represent spurious contributions such as diode shot noise, other instrumental noise, or vibrations of the microscope.* This is impossible because our spectra represent excess power of contracting over rigor muscle.

2. *The oscillations reflect movement artifact.* This is impossible, because cross-linking effectively eliminated shorten-

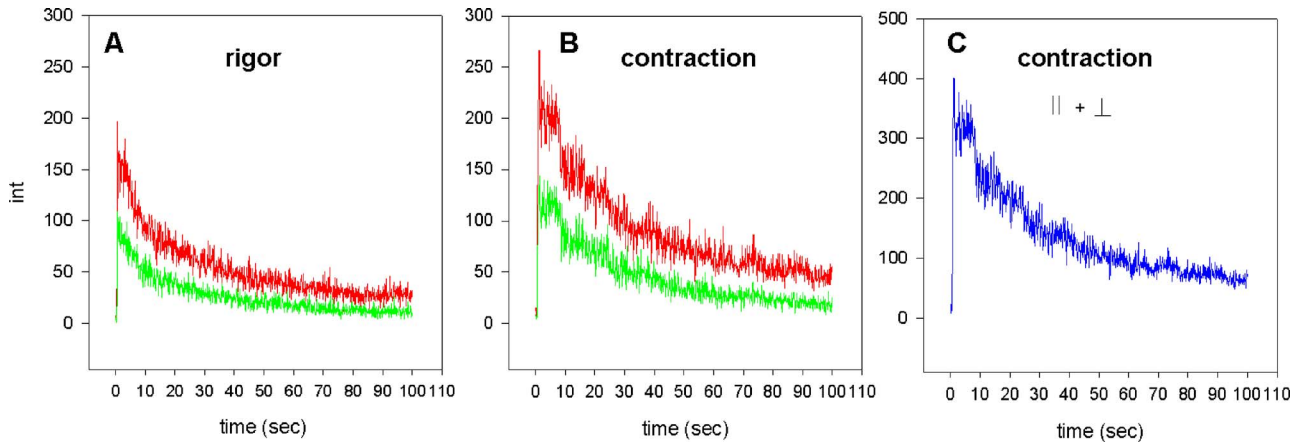


**Fig. 7** Polarization signal obtained from (a) rigor and (b) contracting myofibril. Polarization of the excitation laser beam parallel to the axis of the myofibril. Emission parallel (dark gray) and perpendicular (light gray) to the axis of the myofibril. 0.01- $\mu$ M phalloidin. C-sum of parallel and perpendicular intensities.

ing. 1 to 2% cross-linked cross-bridges probably do not affect the polarized fluorescence power spectrum, since spectrum amplitude is most likely linear with the number of cross-bridges. In all 23 experiments lasting 100 sec, we did not note any shortening or change in the position of the observed overlap zone. We would easily have been able to detect translation of 0.5  $\mu$ m, i.e., to escape detection shortening would have to be less than 5 nm/sec. The distance between actin monomers is 5.5 nm, and 1 in 1000 actins were fluorescently labeled. The translation of 12 monomers would have resulted in light spikes every  $\sim$ 10 sec, well below frequency range of interest. Besides, we measure polarization, so any change in translational motion should not influence the results.

3. *The oscillations result from gradients of ATP concentration.* This is impossible, because ours were steady-state experiments, i.e., contraction was initiated by addition of ATP. Gradients could have been generated when imposing rapid increase in ATP concentration by rapid photolysis of caged ATP, but not in our steady-state experiments.

4. *The oscillations result from photobleaching.* This is unlikely, because photobleaching was eliminated from the analysis by subtracting the dc component before taking the Fourier transform. There are two additional reasons why photobleaching is unlikely to cause excess power in a signal of contracting muscle. First, bleaching results from the stepwise loss of fluorescence of  $\sim$ 12 fluorophores in  $\sim$ 50 sec (e.g., data of Fig. 7). Therefore, frequency associated with bleaching should be  $\sim$ 12/50 sec  $\sim$  0.24 Hz, well below frequency range of interest. Second, fluorescence of rigor myofibrils bleached at about the same rate as fluorescence of contracting myofibrils. Incidentally, adding deoxygenating solution<sup>46</sup> did not slow down photobleaching significantly.

The steps visible in the data of Fig. 7(b) could arise either from photobleaching of rhodamine or reflect rotational motion of the transition moment. We think that the former is the case for the following reasons. First, the intensity steps in both orthogonal components of fluorescence occurred in synchrony, suggesting that they do not reflect rotational motion. Second, steps occurred as well in rigor muscle, where no ro-

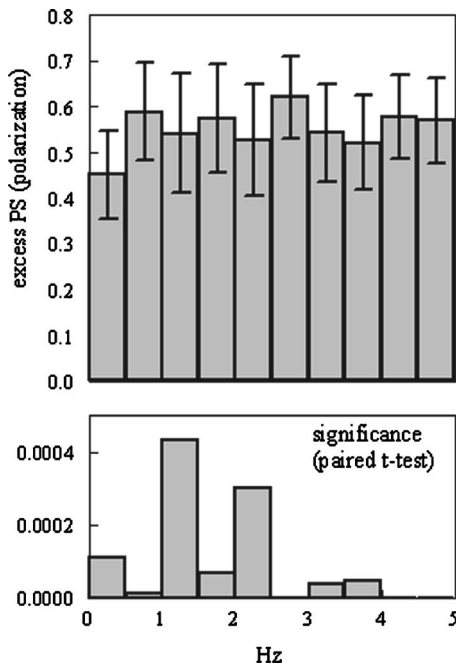


**Fig. 8** (a) Average polarization excess PS and (b) the t-test significance level that data in (a) is not different from zero for experiments on 23 different myofibrils. Error bars show SEM for  $n=23$ .

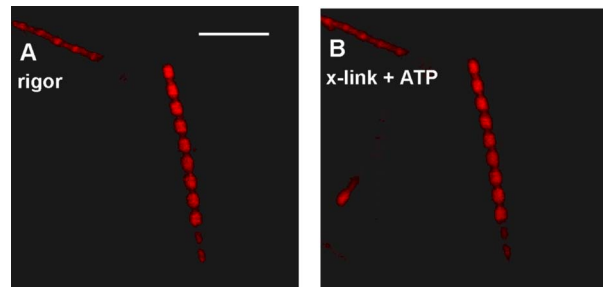


**Fig. 9** Cross-linked myofibrils in (a) rigor solution and (b) after adding contracting solution. Bar=20  $\mu$ m.

tational motion took place. Third, the number of steps roughly corresponded to the number of fluorophores in the detection volume.

Each step lasted  $\sim 10$  sec and led to the loss of  $\sim 100$  cpb [Fig. 7(c)], i.e., we observed  $\sim 10,000$  photons from a fluorophore before it photobleached. The geometrical collection efficiency of the instrument is  $\sim 2\%$ , i.e., a fluorophore emitted a total of  $0.5 \times 10^6$  photons before irreversible bleaching. This is consistent with the known photostability of rhodamine.<sup>47</sup>

The ability to measure the properties of a small number of molecules in a live cell is attractive because it probes molecules in their native crowded environment. This may be responsible for the observations suggesting motility in solution may be accomplished differently than in muscle. Itakura et al.<sup>48</sup> showed that *in vitro*, Dictyostelium S1 devoid of the regulatory domain was able to drive the sliding movement of actin filaments. Tokunaga et al.<sup>49</sup> showed that S1 attached to a glass surface through a flexible random chain moved actin as fast as intact myosin, and that myosin devoid of most of the light chain-binding domain gave the same displacement as intact myosin.<sup>50</sup> Moreover, some data suggest that *in vitro* there is only a loose connection between mechanical and enzymatic events. Thus, the sliding distance in an *in-vitro* assay (near zero load) was reported to be greater than 100 nm during one ATP hydrolysis cycle.<sup>51</sup> Force generation did not coincide with the release of ADP, and instead myosin head *in vitro* was shown to produce force several hundreds of milliseconds after the bound nucleotide was released.<sup>52</sup> In relaxed scallop muscle, the rotation of the regulatory domain was not coupled to a specific step in the ATPase cycle.<sup>53</sup> Our results suggest that individual molecules can be studied in working muscle.

### Acknowledgments

We thank Drs. Z. and I. Gryczynski for helpful suggestions and comments on a manuscript. Supported by R21CA9732 and R01AR048622 (NIAMS) (JB) and by R01AR049277 (NIAMS) and the Mayo Foundation (TPB).

### References

1. A. Houdusse, A. G. Szent-Gyorgyi, and C. Cohen, "Three conformational states of scallop myosin S1," *Proc. Natl. Acad. Sci. U.S.A.* **97**(21), 11238–11243 (2000).
2. D. M. Warshaw, E. Hayes, D. Gaffney, A. M. Lauzon, J. Wu, G. Kennedy, K. Trybus, S. Lowey, and C. Berger, "Myosin conformational states determined by single fluorophore polarization," *Proc. Natl. Acad. Sci. U.S.A.* **95**(14), 8034–8039 (1998).
3. J. N. Forkey, M. E. Quinlan, M. A. Shaw, J. E. Corrie, and Y. E. Goldman, "Three-dimensional structural dynamics of myosin V by single-molecule fluorescence polarization," *Nature (London)* **422**(6930), 399–404 (2003).
4. A. F. Huxley, "A hypothesis for the mechanism of contraction of muscle," *Prog. Biophys. Biophys. Chem.* **7**, 255–318 (1957).
5. C. R. Bagshaw, *Muscle Contraction*, Chapman and Hall, London (1982).
6. A. P. Minton, "Molecular crowding: analysis of effects of high concentrations of inert cosolutes on biochemical equilibria and rates in terms of volume exclusion," *Methods Enzymol.* **295**, 127–149 (1998).
7. T. Arakawa and S. N. Timasheff, "Theory of protein solubility," *Methods Enzymol.* **114**, 49–77 (1985).
8. S. C. Hopkins, C. Sabido-David, J. E. Corrie, M. Irving, and Y. E. Goldman, "Fluorescence polarization transients from rhodamine isomers on the myosin regulatory light chain in skeletal muscle fibers," *Biophys. J.* **74**(6), 3093–3110 (1998).
9. J. Borejdo and I. Akopova, "Orientational changes of cross-bridges during single turnover of ATP," *Biophys. J.* **84**, 2450–2459 (2003).
10. J. Borejdo, A. A. Shepard, I. Akopova, W. Grudzinski, and J. Malicka, "Rotation of the lever-arm of myosin in contracting skeletal muscle fiber measured by two-photon anisotropy," *Biophys. J.* **87**, 3912–3921 (2004).
11. E. H. Hellen, K. Ajtai, and T. P. Burghardt, "Myosin head rotation in muscle fibers measured using polarized fluorescence photobleaching recovery," *J. Fluoresc.* **5**, 355–367 (1995).
12. D. D. Thomas and R. Cooke, "Orientation of spin-labeled myosin heads in glycerinated muscle fibers," *Biophys. J.* **32**, 891–905 (1980).
13. J. Borejdo, O. Assulin, T. Ando, and S. Putnam, "Cross-bridge orientation in skeletal muscle measured by linear dichroism of an extrinsic chromophore," *J. Mol. Biol.* **158**, 391–414 (1982).
14. C. L. Berger, J. S. Craik, D. R. Trentham, J. E. Corrie, and Y. E. Goldman, "Fluorescence polarization of skeletal muscle fibers labeled with rhodamine isomers on the myosin heavy chain," *Biophys. J.* **71**, 3330–3343 (1996).
15. D. Magde, E. L. Elson, and W. W. Webb, "Fluorescence correlation spectroscopy. II. An experimental realization," *Biopolymers* **13**(1), 29–61 (1974).
16. J. Borejdo, S. Putnam, and M. F. Morales, "Fluctuations in polarized fluorescence: evidence that muscle cross-bridges rotate repetitively during contraction," *Proc. Natl. Acad. Sci. U.S.A.* **76**, 6345–6350 (1979).
17. M. Eigen and R. Rigler, "Sorting single molecules: application to diagnostics and evolutionary biotechnology," *Proc. Natl. Acad. Sci. U.S.A.* **91**(13), 5740–5747 (1994).
18. M. J. Levene, J. Koriach, S. W. Turner, M. Foquet, H. G. Craighead, and W. W. Webb, "Zero-mode waveguides for single-molecule analysis at high concentrations," *Science* **299**(5607), 682–686 (2003).
19. B. Hecht, S. B., U. P. Wild, V. Deckert, R. Zenobi, and O. J. F. Martin, "Scanning near-field optical microscopy with aperture probes: fundamentals and applications," *J. Chem. Phys.* **112**, 7761–7774 (2000).
20. R. C. Dunn, "Near-field scanning optical microscopy," *Chem. Rev. (Washington, D.C.)* **99**, 2891–2927 (1999).
21. E. Betzig and R. J. Chichester, "Single molecules observed by near field scanning optical microscopy," *Science* **262**, 1422–1425 (1993).
22. D. Axelrod, "Total internal reflection fluorescence microscopy in cell biology," *Traffic (Oxford, U. K.)* **2**, 764–774 (2001).
23. T. E. Starr and N. L. Thompson, "Local diffusion and concentration of IgG near planar membranes: measurement by total internal reflection with fluorescence correlation spectroscopy," *J. Phys. Chem. B* **106**, 2365–2371 (2002).
24. T. Ruckstuhl and S. Seeger, "Attoliter detection volumes by confocal total-internal-reflection fluorescence microscopy," *Opt. Lett.* **29**(6), 569–571 (2004).
25. T. Ruckstuhl, "Sometimes less is more," *Biophoton.* pp. 48–51 (Sep. 2005).
26. K. Hassler, T. Anhut, R. Rigler, M. Gosch, and T. Lasser, "High count rates with total internal reflection fluorescence correlation spectroscopy," *Biophys. J.* **88**(1), L01-3, Epub 2004 (Nov. 2005).
27. J. Borejdo, A. Shepard, D. Dumka, I. Akopova, J. Talent, A. Malka, and T. P. Burghardt, "Changes in orientation of actin during contraction of muscle," *Biophys. J.* **86**, 2308–2317 (2004).
28. A. E. Bukatina, F. Fuchs, and S. C. Watkins, "A study on the mechanism of phalloidin-induced tension changes in skinned rabbit psoas muscle fibres," *J. Muscle Res. Cell Motil.* **17**(3), 365–371 (1996).
29. E. Prochniewicz-Nakayama, T. Yanagida, and F. Oosawa, "Studies on conformation of F-actin in muscle fibers in the relaxed state, rigor, and during contraction using fluorescent phalloidin," *J. Cell Biol.* **97**, 1663–1667 (1983).
30. D. Szczesna and S. S. Lehrer, "The binding of fluorescent phallotoxins to actin in myofibrils," *J. Muscle Res. Cell Motil.* **14**(6), 594–597 (1993).
31. X. Ao and S. S. Lehrer, "Phalloidin unzips nebulin from thin filaments in skeletal myofibrils," *J. Cell. Sci.* **108**(11), 3397–3403 (1995).
32. C. Herrmann, J. Sleep, P. Chaussepied, F. Travers, and T. Barman, "A structural and kinetic study on myofibrils prevented from shortening by chemical cross-linking," *Biochemistry* **32**(28), 7255–7263 (1993).
33. D. Axelrod, "Total internal reflection fluorescence microscopy," *Methods Cell Biol.* **30**, 245–270 (1989).

34. T. P. Burghardt and N. L. Thompson, "Effect of planar dielectric interfaces on fluorescence emission and detection. Evanescent excitation with high-aperture collection," *Biophys. J.* **46**, 729–737 (1984).
35. E. J. Potma, I. A. van Graas, and G. J. Stienen, "Effects of pH on myofibrillar ATPase activity in fast and slow skeletal muscle fibers of the rabbit," *Biophys. J.* **67**(6), 2404–2410 (1994).
36. T. Wilson, *Confocal Microscopy*, T. Wilson, Ed., pp. 1–64, Academic Press, New York (1990).
37. M. Born and E. Wolf, *Principles of Optics*, Pergamon Press, Oxford (1975).
38. T. P. Burghardt, K. Ajtai, and J. Borejdo, "In situ single-molecule imaging with attoliter detection using total internal reflection confocal microscope," *Biochemistry* **45**, 4058–4068 (2006).
39. O. A. Andreev, R. Takashi, and J. Borejdo, "Fluorescence polarization study of the rigor complexes formed at different degrees of saturation of actin filaments with myosin subfragment-1," *J. Muscle Res. Cell Motil.* **16**, 353–367 (1995).
40. Z. Gryczynski, I. Gryczynski, and J. Lakowicz, "Simple apparatus for polarization sensing of analytes," *Opt. Eng.* **39**(9), 2351–2358 (2000).
41. T. P. Burghardt and N. L. Thompson, "Evanescent intensity of a focused gaussian light beam undergoing total internal reflection in a prism," *Opt. Eng.* **23**(1), 62–67 (1984).
42. D. Magde, E. L. Elson, and W. W. Webb, "Fluorescence correlation spectroscopy. II. An experimental realization," *Biopolymers* **13**(1), 29–61 (1974).
43. D. Mornet, R. Bertrand, P. Pantel, E. Audemard, and R. Kassab, "Structure of the actin-myosin interface," *Nature (London)* **292**(5821), 301–306 (1981).
44. R. W. T. Lymn, E. W. Taylor, "Mechanism of adenosine triphosphate hydrolysis by actomyosin," *Biochemistry* **10**, 4617–4624 (1971).
45. R. Mendelson, M. F. Morales, and J. Botts, "Segmental flexibility of S1 moiety of myosin," *Biochemistry* **12**, 2250–2255 (1973).
46. Y. Harada, K. Sakurada, T. Aoki, D. D. Thomas, and T. Yanagida, "Mechanochemical coupling in actomyosin energy transduction studied by in vitro movement assay," *J. Mol. Biol.* **216**, 49–68 (1990).
47. C. Eggeling, J. Widengren, R. Rigler, and C. A. M. Seidel, "Photobleaching of fluorescent dyes under conditions used for single-molecule detection: evidence of two-step photolysis," *Anal. Chem.* **70**, 2651–2659 (1998).
48. S. Itakura, H. Yamakawa, Y. Y. Toyoshima, A. Ishijima, T. Kojima, Y. Harada, T. Yanagida, T. Wakabayashi, and K. Sutoh, "Force-generating domain of myosin motor," *Biochem. Biophys. Res. Commun.* **196**(3), 1504–1510 (1993).
49. M. Tokunaga, A. Iwane, K. Kitamura, and T. Yanagida, "S1 attachment to a glass surface through a flexible random chain can move actin as fast as intact myosin," *Biophys. J.* **76**, A36 (1999).
50. H. Tanaka, A. Iwane Hikikossi, T. Okamura, S. Morimoto, T. Kusumoto, A. Ishijima, and T. Yanagida, "Role of myosin neck region in generation of movement," *Biophys. J.* **78**, 234A (2000).
51. T. Yanagida, "Loose coupling between chemical and mechanical reactions in actomyosin energy transduction," *Adv. Biophys.* **26**, 75–95 (1990).
52. A. Ishijima, H. Kojima, T. Funatsu, M. Tokunaga, H. Higuchi, H. Tanaka, and T. Yanagida, "Simultaneous observation of individual ATPase and mechanical events by a single myosin molecule during interaction with actin," *Cell* **92**(2), 161–171 (1998).
53. I. Brust-Mascher, L. E. LaConte, J. E. Baker, and D. D. Thomas, "Myosin light-chain domain rotates upon muscle activation but not ATP hydrolysis," *Biochemistry* **38**(39), 12607–12613 (1999).
54. C. Karatzaferi, M. K. Chinn, R. Cooke, K. H. Myburgh, and K. Franks-Skiba, "The force exerted by a muscle cross-bridge depends directly on the strength of the actomyosin bond. Effect of an ADP analog on isometric force and ATPase activity of active muscle fibers," *Biophys. J.* **87**(4), 2532–2544 (2004).